Japanese Journal of Applied Physics
Vol. 45, No. 3B, 2006, pp. 2225–2229

©2006 The Japan Society of Applied Physics

Towards Spin-Polarized Scanning Tunneling Microscopy on Magnetite (110)

Gabriela MARIS*, Lucian JDIRA, Jan G. H. HERMSEN, Shane MURPHY[1], Giuseppe MANAI[1], Igor V. SHVETS[1] and Sylvia SPELLER

Experimental Solid State Physics II, Institute for Molecules and Materials, Toernooiveld 1, Radboud University of Nijmegen, The Netherlands
[1]*SFI Nanoscience Laboratory, Department of Physics, Trinity College, Dublin 2, Ireland*

(Received July 4, 2005; accepted October 24, 2005; published online March 27, 2006)

We study the structure and the magnetic properties of the (110) surfaces of magnetite Fe_3O_4 thin films by scanning tunneling microscopy (STM) and spectroscopy (STS). The STM images show a surface reconstruction consisting of ridges along the [$\bar{1}$10] direction. The data indicate a pure outermost layer followed underneath by a Mg^{2+}-contaminated layer. The metallic and semiconductor-like shapes of the measured current–voltage (I–V) curves indicate different thicknesses of the contaminated layer. While the W tips show in the current map small differences between the tops and valleys of ridges, the antiferromagnetic MnNi tips show a strong contrast at 0.3 and −0.7 V bias voltages. We discuss whether these observations can be related to the detection of spin-polarized current. [DOI: 10.1143/JJAP.45.2225]

KEYWORDS: scanning tunneling microscopy, Fe oxides, surface magnetism, spin polarization

1. Introduction

Magnetite (Fe_3O_4) as a ferrimagnet predicted to be a half metal has a high potential for spin-valve and magnetic recording applications. Thus, the understanding of the structural and magnetic properties of magnetite surfaces down to the atomic scale has attracted considerable research interest. The use of scanning tunneling microscopy/spectroscopy (STM/STS) and spin-polarized STM/STS is of crucial importance in this respect.

The (001) surface of magnetite has been extensively studied by STM both in single-crystal and thin-film forms and several surface terminations have been proposed.[1–5] Magnetic contrast interpretations were given to the STM images of Fe_3O_4(001) and (111) surfaces aquired with spin-selective tips, i.e., ferromagnetic Fe and antiferromagnetic MnNi tips.[6–10] In comparison with the amount of effort in studying the (001) and (111) surfaces, little interest has been given to the (110) surface. STM investigations on this surface have been performed only with a paramagnetic W tip, despite of the predicted termination that contains Fe ions belonging to two different magnetic sublattices. Such an arrangement could give rise to magnetic contrast.[11,12] Furthermore, the (110) surface is predominantly present in the biogenic magnetite crystals found in bacteria and vertebrates.[13–15] These crystals are thought to be involved in magnetoreception, the ability to sense the polarity or the inclination of the earth's magnetic field and to be involved in navigation. Thus peculiar magnetic properties are expected for the (110) orientation. Moreover, spin-dependent transport in materials with a high degree of spin polarization has attracted a lot of research interest due to their high potential for technological applications. Thus, detecting the spin polarization signature of the magnetite surface (which in bulk is predicted to be fully spin-polarized) has importance for devices that employ spin electronic currents. Thus we studied the (110) surface of magnetite.

In this paper, we present a structural study of the (110) surface of Fe_3O_4 thin films down to the atomic scale. We discuss and compare the results of spectroscopy measurements performed with paramagnetic W tips and antiferromagnetic MnNi tips.

Magnetite has an fcc cubic inverse spinel crystal structure with a lattice constant of 8.397 Å.[16] The tetrahedral sites are occupied by Fe^{3+} ions and the octahedral sites are shared between equal amounts of Fe^{3+} and Fe^{2+} ions. The two sublattices formed by the octahedral and the tetrahedral sites couple antiferromagnetically and have different magnetic moments resulting in a net magnetization. The conductance takes place at the octahedral sites due to the continuous hopping between Fe^{2+} and Fe^{3+} ions. Theoretical calculations predict that the bulk transport is 100% spin-polarized.[17–19]

Two types of bulk termination for the (110) surface exist: type A contains both tetrahedrally and octahedrally coordinated Fe ions and type B contains octahedrally coordinated Fe ions (Fig. 1). The type A and type B layers alternate in the bulk with an interlayer spacing of 1.484 Å. The two types of surface are equally polar (+3 and −3) and thus assuming bulk truncations, the surface is expected to be reconstructed.

2. Experimental

The Fe_3O_4(110) thin films used in this study were deposited on MgO(110) substrates by e-beam evaporation from an Fe wire at a growth rate of 5 Å/min. The O pressure was 2×10^{-6} mbar and the substrate temperature during the evaporation was 523 K. Two different annealing procedures

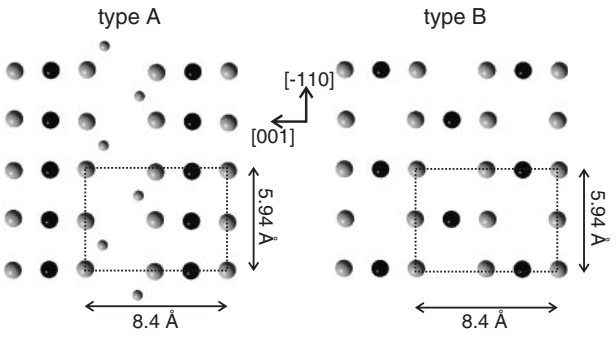

Fig. 1. A and B type (110) layers that alternate in bulk. The surface unit cell is indicated by a rectangle. Large grey circles denote O ions. The tetrahedral and octahedral Fe ions are represented as small grey and large black circles, respectively.

*E-mail address: g.maris@science.ru.nl

applied to two separate films were used to obtain well-ordered surfaces. The first procedure consisted of 30 min annealing at 1000 K in ultrahigh vacuum (UHV). A second film was first annealed at 1000 K in 2×10^{-6} mbar oxygen followed by 10 min annealing at 1000 K in UHV. After preparation, the samples were transferred under UHV conditions in the analysis chamber. The samples were inspected by Auger electron spectroscopy (AES) to estimate the degree of contamination in the surface region. The AES spectra were acquired in the integral [N(E)] mode and were subsequently differentiated. The composition in the surface region was estimated using atom sensitivity factors. The STM/STS measurements were performed at a base pressure below 5×10^{-11} mbar at room temperature with an Omicron UHV STM-1. We have used 20 paramagnetic W tips and 3 antiferromagnetic MnNi tips.[20] Etched W tips were prepared by 15 min sputtering with Ar^+ ions (1 kV) and annealing at 700 K. This preparation resulted in sharp tips with a radius of approximatively 50 nm. Blunt (with radius $>$ 200 nm), clean W tips were subsequently obtained by melting their apex through electron bombardment (by applying 600 V between a W filament and the sharp tip placed 2 mm below the filament). Etched MnNi tips were prepared by 10 min sputtering with Ar^+ ions (1 kV).

3. Results and Discussion

The first film annealed in UHV at 1000 K showed a well-ordered surface consisting of ridges running along the $[\bar{1}10]$ direction with a 25 Å periodicity corresponding to $p(1 \times 4)$ reconstruction.[11,12] For the second film, after the first step of annealing at 2×10^{-6} mbar at 1000 K a well-ordered surface was not obtained, although a tendency for this ordering could be distinguished. The ridge reconstruction was achieved after a second step of annealing at 1000 K in UHV.

From the Auger spectra of the annealed films we derive a contamination level for magnesium of ~5.9%. This content of Mg^{2+} ions is sufficient to play an important role in the observed $p(1 \times 4)$ reconstruction. This is supported by a similar $p(1 \times 4)$ reconstruction observed on a (001) surface of a magnetite thin film grown on MgO after annealing at 880 K,[21] as well as on a natural magnetite single crystal after long annealing at 990 K.[2,5] In both cases, the reconstruction is interpreted as being induced by the contamination of the surface due to the segregation of Mg^{2+} and Ca^{2+} ions, respectively.

The reason that only a tendency for the ridge reconstruction was obtained after annealing in oxygen at 1000 K, while a clear ridge reconstruction was achieved by annealing in UHV at the same temperature is probably related to the balance between Fe, O, and Mg ions necessary for a well-ordered surface. Presumably, when annealing is performed in O, a higher annealing temperature resulting in a higher Mg^{2+} concentration is necessary to obtain ridge reconstruction.

Our STM images acquired with paramagnetic W tips and antiferromagnetic MnNi tips show a surface morphology consisting of terraces with edges perpendicular to the $[\bar{1}10]$ direction. The step heights between terraces are integer multiples of 3.0 ± 0.3 Å [Fig. 2(a)]. This corresponds to the distance between similar layers (A–A or B–B) in the bulk structure. Each terrace ripples in the $[\bar{1}10]$ direction. The

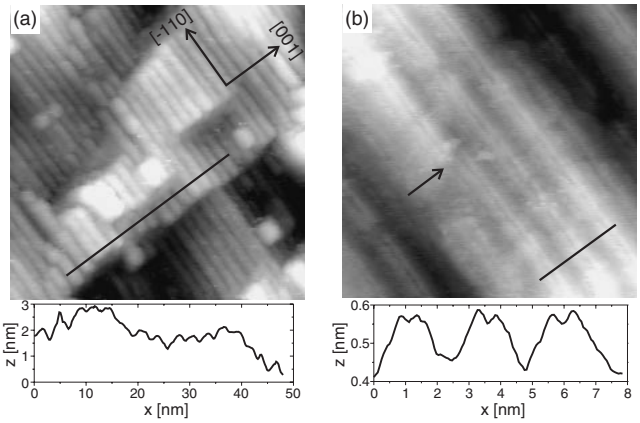

Fig. 2. (a) 700×700 Å^2 STM image showing terrace morphology with ridges along the $[\bar{1}10]$ direction separated by 25 Å. The image was taken with a W tip at a tunneling current of 0.85 nA and a bias voltage of 0.5 V. The line profile along the [001] direction shows the 25 Å periodicity of the ridges. (b) 200×200 Å^2 STM image showing resolution on top of the ridges. The image was taken with a MnNi tip at a tunneling current of 0.5 nA and a bias voltage of 1 V. The line profile along the [001] direction shows a 1.5 Å vertical corrugation perpendicular to the ridges. The defect line along which one of the ridges shifts with 1/2[001] is indicated by an arrow.

periodicity of the ridges is mostly 25.0 ± 0.3 Å. This periodicity corresponds to threefold the bulk lattice constant (8.4 Å). Sometimes we observe a 34.0 ± 0.3 Å periodicity in agreement with fourfold the bulk lattice constant. The vertical corrugation perpendicular to the ridges is 1.5 ± 0.3 Å which corresponds to a quarter of the bulk lattice constant. Thus, the ridge morphology of a terrace can be viewed as a bulk layer which shifts up and down periodically with a shift vector of 1/4[110].

On the top of the ridges we resolved rows running along the $[\bar{1}10]$ direction. In Fig. 2(b) we present an image taken with a MnNi tip showing on top of the ridges two rows separated by 6.0 ± 0.3 Å. Images taken with seven W tips and two MnNi tips showed double rows on top of the ridges with distances varying between 6.0 ± 0.3 Å and 12.0 ± 0.3 Å. Shifts along the [001] direction [as the one indicated by an arrow in Fig. 2(b)] with shift vectors of 1/2[001] are sometimes observed.

Using a very clean W tip obtained by melting its top through electron bombardment, we observe a significant improvement in the resolution of the STM images. In Fig. 3(a) we show an example of such an image where the top of one ridge with a width of 12.0 ± 0.3 Å is very well resolved. This tip images periodicity along both the [001] and $[\bar{1}10]$ directions. The smallest distance between two atoms imaged along the [001] direction is 2.1 ± 0.3 Å. This distance is in good agreement with the bulk Fe–O distance. Along the $[\bar{1}10]$ direction, the periodicity is 3.0 ± 0.3 Å which corresponds to the 2.97 Å distance between two consecutive oxygen ions or two consecutive octahedral iron ions of the bulk A layer (see Fig. 1). We attribute the indentation in the middle of the top of the ridge to the spacing between the tetrahedral Fe^{3+} ions rows of the bulk A-layer. This indented line feature is often resolved in our STM images using different W and MnNi tips [Fig. 2(b)]. Considering a bulk A-layer truncation, the imaged rows of atoms are attributed to octahedral Fe and O sites as indicated

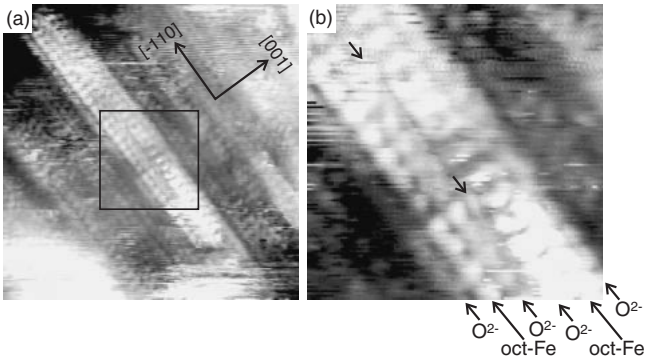

Fig. 3. (a) $90 \times 90\,\text{Å}^2$ atomically resolved STM image showing periodicity along [$\bar{1}$10] and [001] directions. The image was acquired with a clean blunt W tip at a tunneling current of 0.76 nA and at a bias voltage of 1.5 V. (b) $30 \times 30\,\text{Å}^2$ zoom in the area indicated by a square in (a). The O ion rows and octahedral Fe ion rows are indicated by arrows outside the image. The tetrahedral Fe ions are indicted by arrows inside the image.

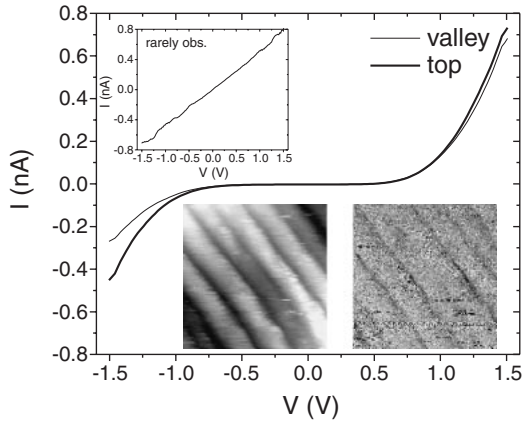

Fig. 4. Semiconductor-like shapes of *I–V* curves measured with W tip on top and on valleys of ridges. Each curve is obtained by averaging over large, contaminated free areas of tops and valleys of ridges. Lower inset: $150 \times 150\,\text{Å}^2$ topography and the corresponding *I–V* map showing a small contrast correlated with ridge structure. The bias voltage for *I–V* map is 1.4 V. The tip-sample distance was set by stabilizing a tunneling current of 0.73 nA and a bias voltage of 1.5 V. Upper inset: ohmic like shapes of *I–V* characteristics measured with clean blunt W tip. As the *I–V* curves taken in the valleys and on the tops of the ripples differ only insignificantly, we show the *I–V* curve obtained by averaging over both valley and top areas. The tip sample was set by stabilizing a 0.65 nA current at a bias voltage of 1.5 V.

by the arrows outside the image in Fig. 3(b). The fact that both octahedral Fe rows and O rows are seen as bright features explains the different distances measured between the two rows that we typically observe on top of the ridges. The tetrahedral Fe^{3+} ions are sometimes observed. The arrows inside the image shown in Fig. 3(b) indicate sites of tetrahedral Fe^{3+} ions. Although the valleys are less well resolved than the tops of the ridges, we can still identify in the valleys a $3.0 \pm 0.3\,\text{Å}$ periodicity along the [$\bar{1}$10] direction corresponding to a bulk A layer.

Remarkably, the sites of the O atoms are imaged as bright features. This contradicts the band structure calculations of bulk Fe_3O_4 indicating that the O_p orbitals lie well below the Fermi energy.[19] However, the Mg^{2+} ions present at the surface can influence the position of the O_{3s} orbitals. Indeed, electronic structure calculations show that the conduction band of MgO has predominantly O_{3s} characteristics.[22] On the basis of this argument we predict that the bright appearance of the O ions in our STM images is caused by the presence of Mg^{2+} ions in their vicinity. While in this scenario, O ions would appear bright, the Mg^{2+} ions would appear as depressions. As no depressions are visible in our STM images that could be attributed to the Mg^{2+} ions, we conclude that they are located in the layer underneath the outermost layer. This underneath layer is of the B type and the Mg^{2+} ions can intercalate at the interstitial positions of octahedral Fe ion rows (see Fig. 1). A similar intercalation of the Ca^{2+} ions is proposed for the $p(1 \times 4)$ reconstructed (001) surface of a Fe_3O_4 natural crystal.[5] As the Auger signal is sensitive to a few monolayers, the magnesium peak observed in the spectra can originate from the Mg^{2+} ions located underneath the outermost layer. Thus our interpretation is in good agreement with the AES measurements.

On the basis of these well-resolved images we conclude that the surface reconstruction is of the A type, containing both octahedral and tetrahedral Fe ions. As the bulk A-layer is polar, charge neutrality can be obtained by vacancies at the tetrahedral sites. However, for a full description of a stable non polar surface, the charges of the deeper layers have to be included.

The conductivity characteristic of the $Fe_3O_4(110)$ surface is analyzed by STS. Two types of shape for the current–voltage (*I–V*) characteristics are observed in the STS measurements performed with the W tips. The majority of measurements show semiconductor-like *I–V* curves also at low tunneling resistances (Fig. 4). However, approximately 10% of the time we have observed ohmic-like shapes for the *I–V* curves (upper inset of Fig. 4). At first we have speculated that the purity of the tip influences the type of shape for the *I–V* characteristics. However, new experiments excluded this possibility as with the same tip we measured both types of shapes in different regions of the sample. We believe that the difference in the *I–V* shape is related to the variable thickness of the Mg contaminated layer.[21] Thus, if Mg ions are located only in one monolayer underneath the outermost layer, the *I–V* curves can still show metallic-like shapes. However, the presence of Mg in several monolayers will result in a sufficiently thick semiconducting layer and the corresponding *I–V* curves will have semiconductor-like shapes. The variable thickness of the Mg-contaminated layer is probably related to the non uniform thickness of our film.

The small contrast between tops and the valleys of the ridges (lower inset of Fig. 4) is typically measured with W tips. The origin of this contrast can be chemical or could be related to defects in the surface structure. The increased contrast at large negative biases is due to the choice of the set-point bias voltage.

At 0.3 and -0.7 V bias voltages, the STS measurements performed with an antiferromagnetic MnNi tip show large differences between the conductivity in the valleys and the conductivity on the tops of the ridges. The STM image and the corresponding current map at 0.6 V bias voltage are presented in the inset of Fig. 5. The strong dark-bright contrast correlates to the ridge structure such that the bright and dark zones correspond to the valleys and tops of the ridges, respectively. Figure 5 shows the dI/dV curves

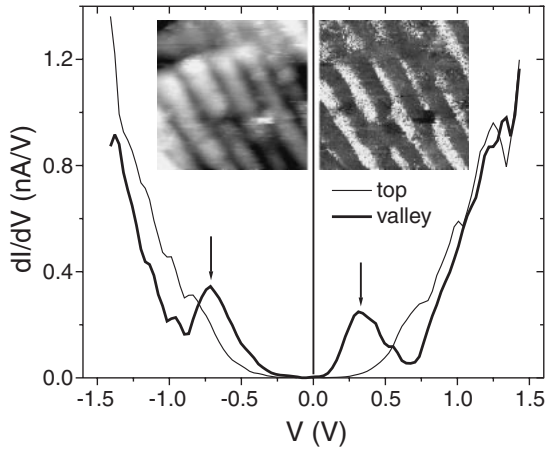

Fig. 5. Derivatives of the *I–V* curves obtained with a MnNi tip on the tops and the valleys of the ridges. Each curve is the average over approximately hundred single curves. The pronounced features at 0.3 and −0.7 V present in the valleys are indicated by arrows. Inset: 150 × 150 Å^2 STM image and corresponding current map taken with MnNi tip and showing strong contrast between tops and valleys of ridges. The bias voltage for this map is 0.6 V. The tip sample distance was set by stabilizing a tunneling current of 0.57 nA and a bias voltage of 1.5 V.

measured in the valleys and on the tops of the ridges. The two pronounced features indicated by arrows at 0.3 and −0.7 V are present only in the valleys and have never been observed in the dI/dV curves measured with a W tip. Although less pronounced, a different MnNi tip shows similar features at 0.3 and −0.7 V, strengthening the validity of these results. The small contrast between the valleys and the tops of the ridges at large biases, i.e., < -1 V and > 1 V is of the same magnitude as the one typically measured with the paramagnetic W tip.

An explanation of the magnetic origin of the pronounced features measured with the MnNi tip can be given by making an analogy between the antiphase boundaries (APB) of the Fe_3O_4(001) thin films and the ridge boundaries (RB) delimiting the tops from the valleys in the (110) films. The APBs in the (001)Fe_3O_4 thin films are formed as a result of the mismatch between the film and the MgO substrate.[23–25] Both APB and RB show 1/4[110] shift vectors. It was shown that the magnetic coupling across the APBs in (001) films can be antiferromagnetic. Similarly, the RB could trigger an antiferromagnetic coupling between the tops and valleys of the ripples. In such a scenario, if the sample magnetization is not orthogonal to the tip magnetization, a magnetic contrast is expected. However, at the moment we cannot exclude the contribution of the tip density of states to the observed contrast. Spin-selective features should also be present in spin-integrated spectroscopy curves. Nevertheless, the combination of tip and sample materials can lead to emphasis or suppression of features, e.g., magnetochemistry. To distinguish the magnetic contrast from other contributions, the application of a magnetic field is crucial. Switching the contrast by applying a magnetic field would give clear proof of spin-polarized current detection. Moreover, extra investigations are necessary for determining the orientation of the surface magnetization. By knowing this, magnetic tips can be prepared in a controlled way with a high probability of spin-polarized current detection.

4. Conclusions

The STM study on a magnetite (110) surface indicates a morphology consisting of terraces that ripple in the [$\bar{1}$10] direction. Although the Mg^{2+} ions segregating from the substrate at the surface of the film are involved in the observed reconstruction, our STM images provide evidence of a contaminations free outermost layer. Atomically resolved images taken with a clean blunt W tip resolves periodicity in [$\bar{1}$10] and [001] directions in agreement with a bulk A-type layer containing both octahedral and tetrahedral Fe ions. The O ions are imaged as bright features indicating the presence of Mg^{2+} ions in the layer underneath the outermost layer.

The STS measurements using paramagnetic W and antiferromagnetic MnNi tips show two types of *I–V* characteristic. When the Mg^{2+} contamination is restricted to one monolayer ohmic like *I–V* characteristics are obtained. However, the majority of the measured *I–V* curves maintain a semiconductor-like shape down to low tunneling resistances indicating a contaminated layer thicker than one monolayer. A small contrast between the tops and valleys of the ripples is typically observed in the current map measured with the W tips. The MnNi tips show in the current map a strong dark-bright contrast correlated with the ridge structure. The origin of this contrast can be attributed to magnetism. However, at the moment we cannot exclude the contribution of the tip density of states.

Acknowledgments

The authors would like to thank Professor R. A. de Groot and B. Hulsken for helpful discussions. This study was supported by the ASPRINT European project (NMP-CT-2003-001601) and by NanoNed, the Dutch nanotechnology programme of the Ministry of Economic Affairs.

1) J. M. Gaines, P. J. H. Bloemen, J. T. Kohlhepp, C. W. T. Bulle-Lieuwma, R. M. Wolf, A. Reinders, R. M. Jungblut, P. A. A. van der Heijden, J. T. W. M. Eemeren, J. aan de Stegge and W. J. M. de Jonge: Surf. Sci. **373** (1997) 85.
2) C. Seoighe, J. Naumann and I. V. Shvets: Surf. Sci. **440** (1999) 116.
3) B. Stanka, W. Hebenstreit, U. Diebold and S. A. Chambers: Surf. Sci. **448** (2000) 49.
4) S. A. Chambers, S. Thevuthasan and S. A. Joyce: Surf. Sci. Lett. **450** (2000) L273.
5) S. F. Ceballos, G. Mariotto, K. Jordan, S. Murphy, C. Seoighe and I. V. Shvets: Surf. Sci. **548** (2004) 106.
6) R. Wiesendanger, I. V. Shvets, D. Bürgler, G. Tarrach, H. J. Güntherodt, J. M. D. Coey and S. Gräser: Science **255** (1992) 583.
7) G. Mariotto, S. Murphy and I. V. Shvets: Phys. Rev. B **66** (2002) 245426.
8) I. V. Shvets, G. Mariotto, K. Jordan, N. Berdunov, R. Kantos and S. Murphy: Phys. Rev. B **70** (2004) 155406.
9) K. Jordan, G. Mariotto, S. F. Ceballos, S. Murphy and I. V. Shvets: J. Magn. Magn. Mater. **290** (2005) 1029.
10) N. Berdunov, S. Murphy, G. Mariotto and I. V. Shvets: Phys. Rev. Lett. **93** (2004) 057201.
11) R. Jansen, V. A. M. Brabers and H. van Kempen: Surf. Sci. **328** (1995) 237.
12) R. Jansen, R. M. Wolf and H. van Kempen: J. Vac. Sci. Technol. B **14** (1996) 1173.
13) R. E. Dunin-Borkowski, M. R. McCartney, R. B. Frankel, D. A. Bazylinski, M. Pósfai and P. R. Buseck: Science **282** (1998) 1868.
14) C. E. Diebel, R. Proksch, C. R. Greenk, P. Neilson and M. M. Walker:

Nature **406** (2000) 299.
15) D. A. Bazylinski and R. B. Frankel: Nat. Rev. Microbiol. **2** (2004) 217.
16) R. W. G. Wyckoff: *Crystal Structures* (Krieger, Malabar, 1982) 2nd ed., Vols. 1–3.
17) A. Yanase and N. Hamada: J. Phys. Soc. Jpn. **53** (1984) 312.
18) A. Yanase and N. Hamada: J. Phys. Soc. Jpn. **68** (1999) 1607.
19) Z. Zhang and S. Satphaty: Phys. Rev. B **44** (1991) 13319.
20) S. F. Ceballos, G. Mariotto, S. Murphy and I. V. Shvets: Surf. Sci. **523** (2003) 131.
21) J. F. Anderson, M. Kuhn, H. Diebold, K, Shaw, P. Stoyanov and D. Lind: Phys. Rev. B **56** (1997) 9902.
22) P. K. Boer and R. A. de Groot: J. Phys.: Condens. Matter **10** (1998) 10241.
23) D. T. Margulies, F. T. Parker, M. L. Rudee, F. E. Spada, J. N. Chapman, P. R. Aitchison and A. E. Berkowitz: Phys. Rev. Lett. **79** (1997) 5162.
24) F. C. Voogt, T. T. M. Palstra, L. Niesen, O. C. Rogojanu, M. A. James and T. Hibma: Phys. Rev. B **57** (1998) R8107.
25) T. Hibma, F. C. Voogt. L. Niesen, P. A. A. van der Heijden, W. J. M. de Jonge, J. J. T. M. Donkers and P. J. van der Zaag: J. Appl. Phys. **85** (1999) 5291.